

Supporting Information

**Intermolecular Interactions and Protein Dynamics by Solid-State NMR Spectroscopy**

*Jonathan M. Lamley, Carl Öster, Rebecca A. Stevens, and Józef R. Lewandowski\**

anie\_201509168\_sm\_miscellaneous\_information.pdf

## Experimental Section

Deuterated [ $^{13}\text{C}$ ,  $^{15}\text{N}$ ]-labeled GB1 (T2Q) was expressed in *E.coli* BL21(DE3) after one cycle of adaptation to  $\text{D}_2\text{O}$  in a 50 mL pre-culture. The production was carried out in a 3.6 L fermenter using 1 L  $\text{D}_2\text{O}$  M9 minimal media with 6 g  $^{13}\text{C}$ -glucose and 1.5 g  $^{15}\text{NH}_4\text{Cl}$ . The final yield after cell rupture by heating to 75 °C and HPLC purification (RP HPLC column, Jupiter 10 mm  $\text{C}_4$  300 Å) was 152 mg. The level of deuteration was approximately 87%, estimated from solution-state 1D NMR spectra. After lyophilization, the final buffer (10 mL) was adjusted by dialysis against 4 x 1 L 50 mM sodium phosphate, pH 5.5. Lyophilized IgG from human serum was purchased from Sigma-Aldrich. The complex sample was prepared for solid-state NMR by mixing 0.3 mM GB1 and 0.15 mM IgG solutions (2:1 molar ratio; note that in later experiments we used 1:1 molar ratio to the same effect), which resulted in instantaneous precipitation of the complex. The resulting precipitate was centrifuged into a Bruker 1.3 mm NMR rotor. Note that in contrast to several studies that rely on sedimentation by ultracentrifugation for preparing sample of a complex in the case of GB1:IgG complex precipitation occurs spontaneously without any application of centrifugal force. Thus as studied here the complex *is not a sediment but a precipitate*, which is a direct consequence of bivalent nature of interaction of GB1 with IgG. Here centrifugation is a means for mechanical transfer of already formed solid-state sample and not as a way of preparing the sample. The amount of GB1 in the final sample was estimated to be on the order of 8 nanomoles (or ~50  $\mu\text{g}$  of protein).

GB1 was also crystallized from a 10 mg/mL solution with the aid of a precipitant of 2:1 2-methylpentane-2,4-diol:propan-2-ol.<sup>[1]</sup> The resulting nanocrystals were then centrifuged into a Bruker 1.3 mm rotor. The amount of GB1 in the final sample was estimated to be on the order of 310 nanomoles (or ~2 mg of protein).

All solid-state NMR spectra shown, except for  $^{15}\text{N}$   $R_{1\rho}$  relaxation dispersion on crystalline GB1, were recorded at 850 MHz  $^1\text{H}$  Larmor frequency with a Bruker Avance III spectrometer, with a Bruker 1.3 mm triple resonance probe operating at a magic-angle spinning (MAS) frequency of 60 kHz.  $^{15}\text{N}$   $R_{1\rho}$  relaxation dispersion experiments on crystalline GB1 were recorded at 600 MHz  $^1\text{H}$  Larmor frequency with a Bruker Avance II+ spectrometer, with a Bruker 1.3 mm triple resonance probe operating at an MAS frequency of 50 kHz. The rotor caps were sealed with a silicone-based glue to eliminate water leakage, while a Bruker BCU-X cooling unit was used to regulate the internal sample temperature to  $27 \pm 1$  °C (measured from the chemical shift of water with respect to DSS; Bruker macro for calibrating the sample temperature can be downloaded from the authors' website).  $^{15}\text{N}$   $R_{1\rho}$  rates in the complex were measured by recording a series of  $^{15}\text{N}$ - $^1\text{H}$  correlation spectra using the proton-detected pulse sequence shown in SI Fig.1, where the spin-lock duration,  $\tau$ , is incremented between full experiments.

The nutation frequencies for all the spin lock fields used for  $^{15}\text{N}$   $R_{1\rho}$  measurements were determined using nutation experiments.

For  $^{15}\text{N}$   $R_{1\rho}$  measurements on the complex at 60 kHz spinning, double quantum cross-polarization (CP) contact times were 1 ms ( $^1\text{H}$ - $^{15}\text{N}$ ) and 0.4 ms ( $^{15}\text{N}$ - $^1\text{H}$ ), with nutation frequencies of 10 kHz and ~50 kHz for  $^{15}\text{N}$  and  $^1\text{H}$  (with 5% tangential sweep) respectively. Relaxation series were collected with spin-lock nutation frequencies of both 17 kHz and 2.5 kHz. For each experiment within the 17 kHz series, 224 scans of 74  $t_1$  increments were taken (experimental time ~85 h), while for the 2.5 kHz series 96 scans of 64  $t_1$  increments were taken per experiment (experimental time ~10 h). Recycle delays were 2 s.

For  $^{15}\text{N}$   $R_{1\rho}$  measurements on the complex at 52 kHz spinning, double quantum cross-polarization (CP) contact times were 1.3 ms ( $^1\text{H}$ - $^{15}\text{N}$ ) and 0.75 ms ( $^{15}\text{N}$ - $^1\text{H}$ ), with nutation frequencies of 10 kHz and ~42 kHz for  $^{15}\text{N}$  and  $^1\text{H}$  (with 5% tangential sweep) respectively. Relaxation series were collected with spin-lock nutation frequencies of 13.1 kHz. 168 scans of 46  $t_1$  increments were taken (experimental time ~45 h). Recycle delays were 2 s. Data was acquired in an interleaved fashion.

For  $^{15}\text{N}$   $R_{1\rho}$  measurements on the complex at 45 kHz spinning, double quantum cross-polarization (CP) contact times were 1.2 ms ( $^1\text{H}$ - $^{15}\text{N}$ ) and 0.5 ms ( $^{15}\text{N}$ - $^1\text{H}$ ), with nutation frequencies of 8 kHz and ~37 and ~53 kHz for  $^{15}\text{N}$  and  $^1\text{H}$  (with 5% tangential sweep) respectively. Relaxation series were collected with spin-lock nutation frequencies of 13 kHz. 160 scans of 68  $t_1$  increments were taken (experimental time ~63 h). Recycle delays were 2 s. Data was acquired in an interleaved fashion.

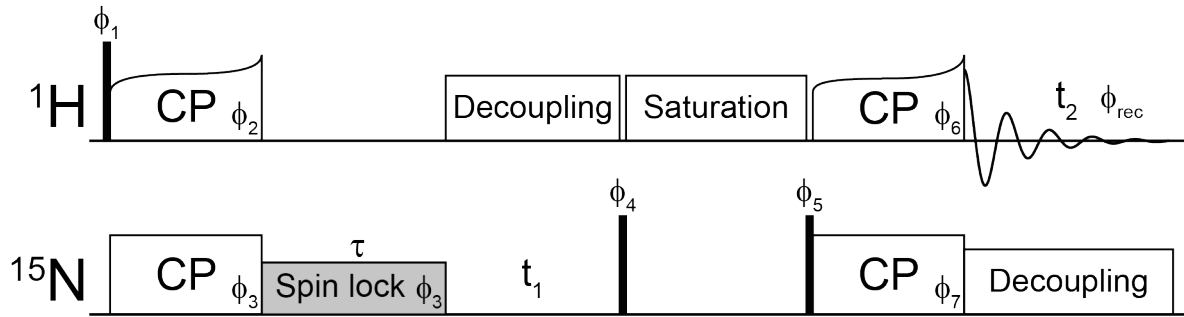
For  $^{15}\text{N}$   $R_1$  measurements on the complex at 60 kHz spinning, double quantum cross-polarization (CP) contact times were 1.2 ms ( $^1\text{H}$ - $^{15}\text{N}$ ) and 0.85 ms ( $^{15}\text{N}$ - $^1\text{H}$ ), with nutation frequencies of 10 kHz and ~50 kHz for  $^{15}\text{N}$  and  $^1\text{H}$  respectively. The relaxation curve was sampled with five points with relaxation delays between 2 ms and 24 s. 128 scans of 56  $t_1$  increments were taken (experimental time 118.5 h). Recycle delays were 2 s.

For  $^{15}\text{N}$   $R_{1\rho}$  relaxation dispersion on crystalline GB1, a series of interleaved  $^{15}\text{N}$   $R_{1\rho}$  measurements were performed at spin-lock frequencies 1.95, 2.44, 3, 4, 5, 6 and 8 kHz. Each  $R_{1\rho}$  curve was sampled using 10-12 points with spin-locks up to 0.5 s. 4 scans of 70  $t_1$  increments were collected, with a recycle delay of 2 s (total experimental time X).  $^1\text{H}$ - $^{15}\text{N}$  and  $^{15}\text{N}$ - $^1\text{H}$  CP contact times were 1.5 and 1.0 ms, respectively, with nutation frequencies of 10 kHz ( $^{15}\text{N}$ ) and ~40 kHz ( $^1\text{H}$ ).

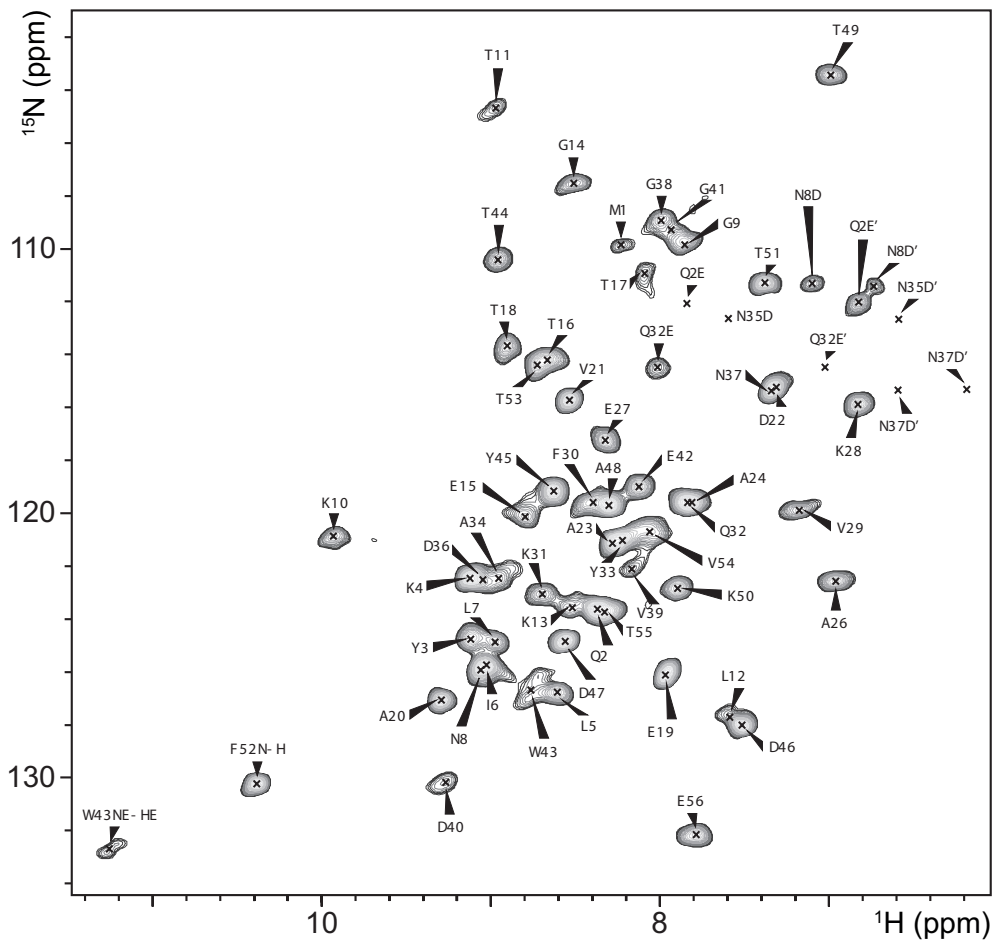
For  $^{15}\text{N}$   $R_1$  measurements on crystalline GB1 at 60 kHz spinning, double quantum cross-polarization (CP) contact times were 0.6 ms ( $^1\text{H}$ - $^{15}\text{N}$ ) and 0.7 ms ( $^{15}\text{N}$ - $^1\text{H}$ ), with nutation frequencies of 10 kHz and ~50 kHz for  $^{15}\text{N}$  and  $^1\text{H}$  respectively. The relaxation curve was sampled with ten points with relaxation delays between 2 ms and 27 s. 16 scans of 98  $t_1$  increments were taken (experimental time 42 h). Recycle delays were 2 s.

For all experiments, 10 kHz WALTZ-16 heteronuclear decoupling was applied to  $^1\text{H}$  during  $^{15}\text{N}$  evolution, and to  $^{15}\text{N}$  during direct  $^1\text{H}$  acquisition, while suppression of the  $^1\text{H}$  signal of water was achieved by saturation with 200 ms (for the complex) or 50 ms (for the crystals) of slpTPPM  $^1\text{H}$  decoupling<sup>[2]</sup> applied at an amplitude of  $\frac{1}{4}$  of the MAS frequency. In all experiments, hard pulses were applied at nutation frequencies of 100 kHz ( $^1\text{H}$  and  $^{13}\text{C}$ ) and 50 or 83.3 kHz ( $^{15}\text{N}$ ). Quadrature detection was achieved using the States-TPPI method. Each of the spin-lock frequencies were determined using nutation experiments.

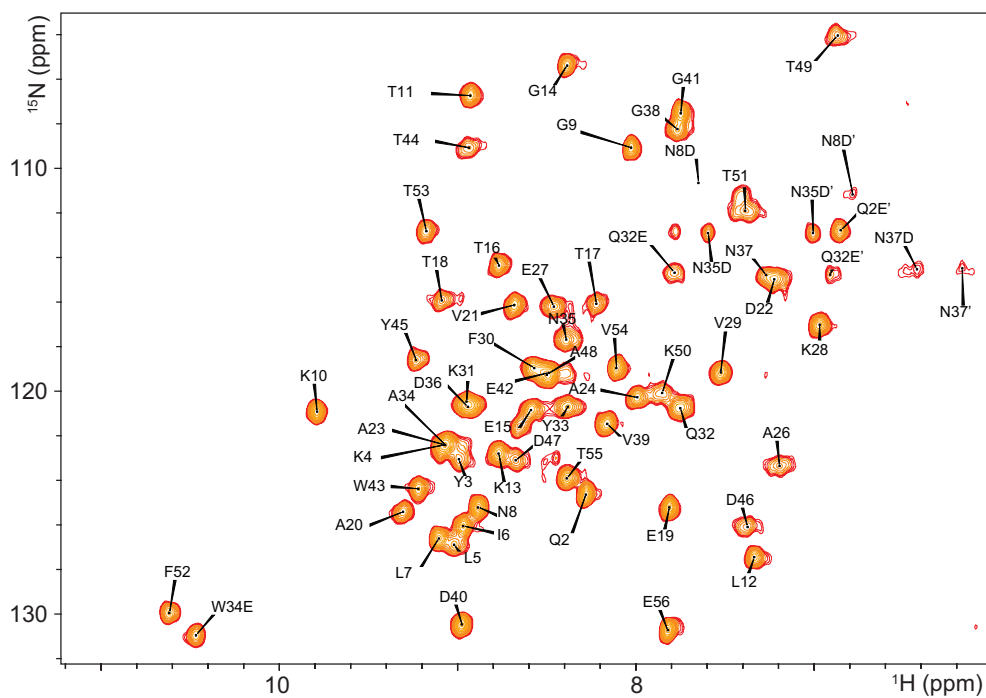
TopSpin 3.2 and CcpNmr Analysis 2.2.2 were used to process spectra and analyze the relaxation data, which was subsequently fitted using Origin 9.1. Fig.2-3 were produced using the UCSF Chimera package<sup>[3]</sup>.



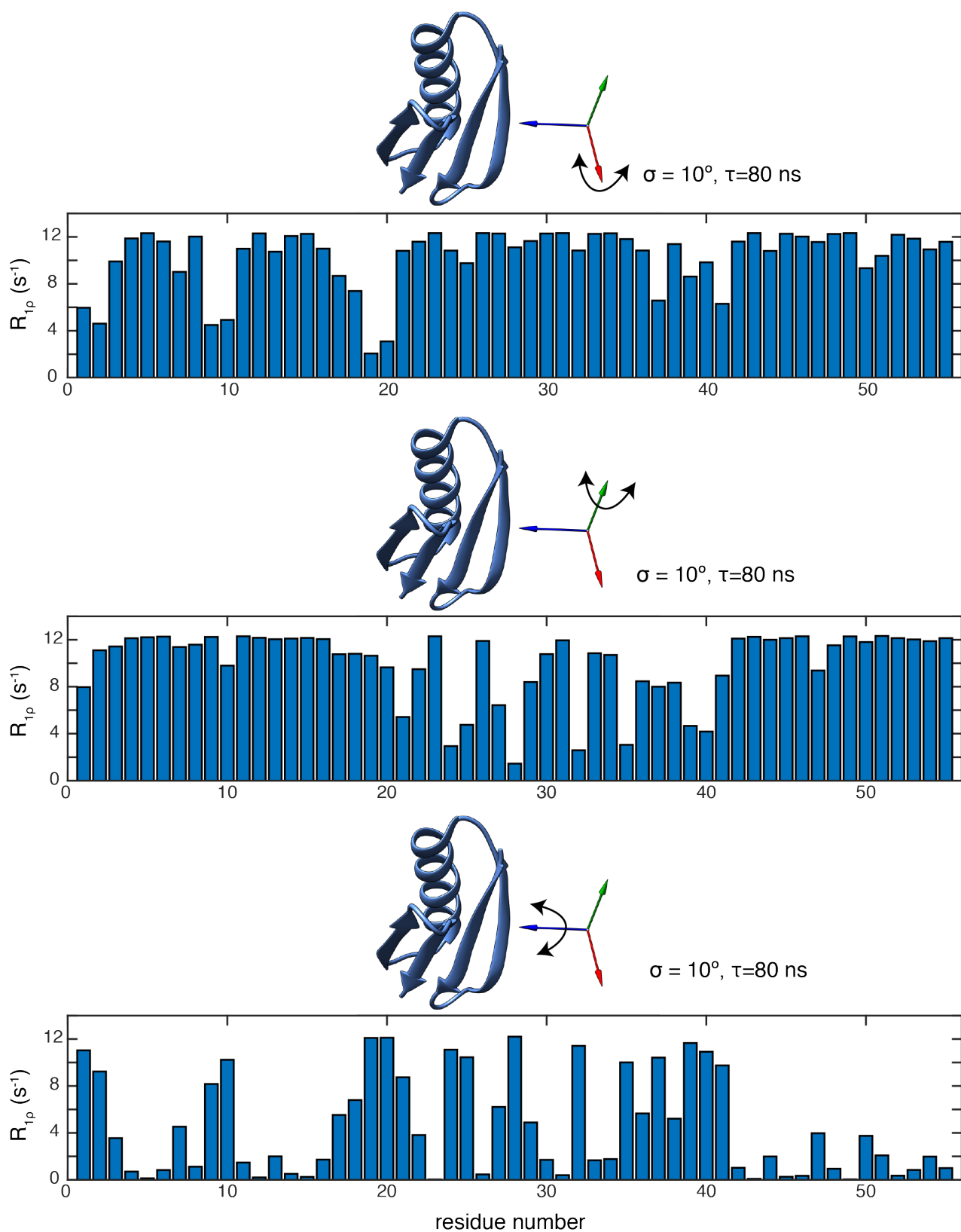
**Figure S1.** Pulse sequence used for measuring  $^{15}\text{N}$   $R_1$  rates in the GB1:IgG complex, where direct proton detection offers a crucial enhancement in sensitivity compared to nitrogen or carbon detection. Hard  $\pi/2$  pulses are shown as black rectangles. The spin-lock pulse, colored in gray, is incremented (length  $\tau$ ) between experiments to follow the  $R_1$  relaxation of the  $^{15}\text{N}$  nuclei. Phase cycling:  $\phi_1=(+y)$ ,  $\phi_2=(+y +y +y +y -y -y -y -y)$ ,  $\phi_3=(+x)$ ,  $\phi_4=-\phi_5=(+x +x -x -x)$ ,  $\phi_6=(+y +y -y -y)$ ,  $\phi_7=(+y -y +y -y)$ ,  $\phi_{\text{rec}}=(+y -y -y +y -y +y +y -y)$ .



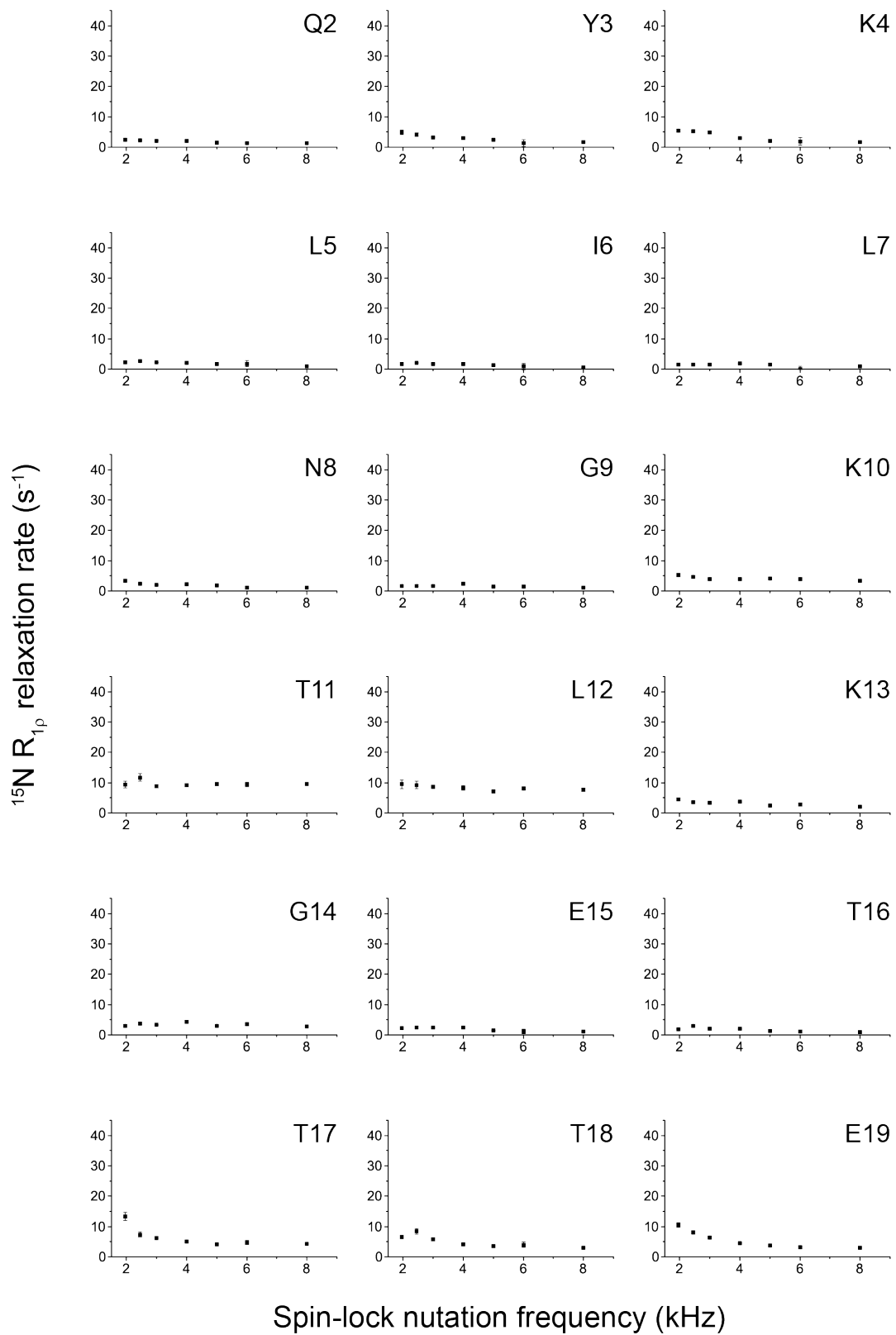
**Figure S2.** Assigned 2D  $^{15}\text{N}$ - $^1\text{H}$  spectrum of deuterated (full-protonated at exchangeable sites)  $[\text{U-}^{13}\text{C}, ^{15}\text{N}]\text{GB1}$  in complex with natural abundance full-length human IgG, recorded at a  $^1\text{H}$  Larmor frequency of 850 MHz and at an MAS frequency of 60 kHz.

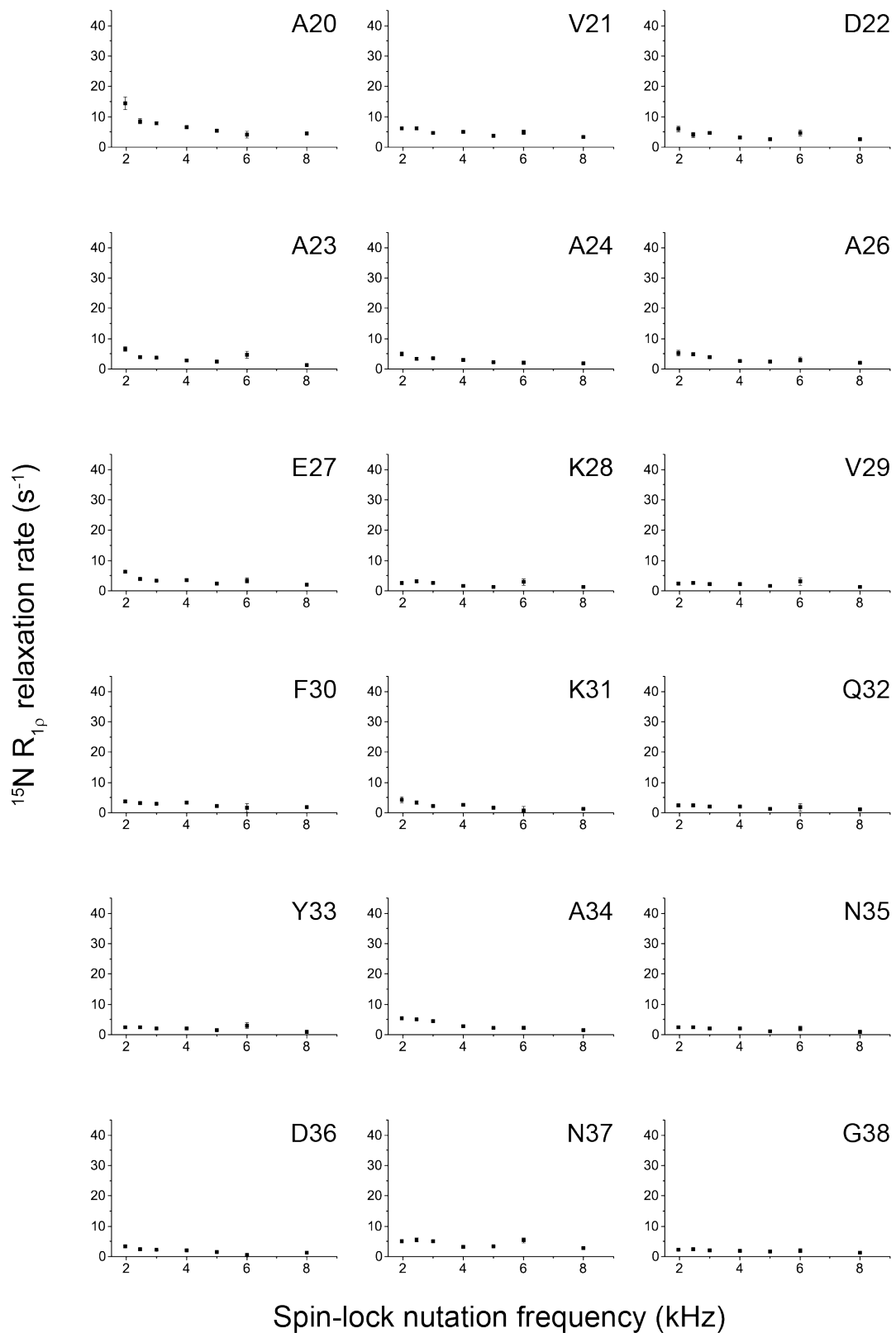


**Figure S3.** Assigned 2D  $^{15}\text{N}$ - $^1\text{H}$  spectrum of deuterated (full-protonated at exchangeable sites) crystalline  $[\text{U-}^{13}\text{C}, ^{15}\text{N}]\text{GB1}$ , recorded at a  $^1\text{H}$  Larmor frequency of 850 MHz and at an MAS frequency of 60 kHz.



**Figure S4.** Simulated  $^{15}\text{N}$   $R_{1\rho}$  rates for overall anisotropic motion of GB1 about three different motional axes (inertia axes for GB1 structure PDB ID: 2qmt<sup>[4]</sup>). The rates were simulated using 3D GAF<sup>[5]</sup> for a 10 degree fluctuation against the indicated axes, with a correlation time of 80 ns at 850  $^1\text{H}$  Larmor frequency. Both  $^{15}\text{N}$ - $^1\text{H}$  dipolar and  $^{15}\text{N}$  CSA contributions were considered. For  $^{15}\text{N}$  CSA the following parameters were assumed:  $\sigma_{11}=231.4$  ppm,  $\sigma_{22} = 80.6$  ppm and  $\sigma_{33}=54.0$  ppm.





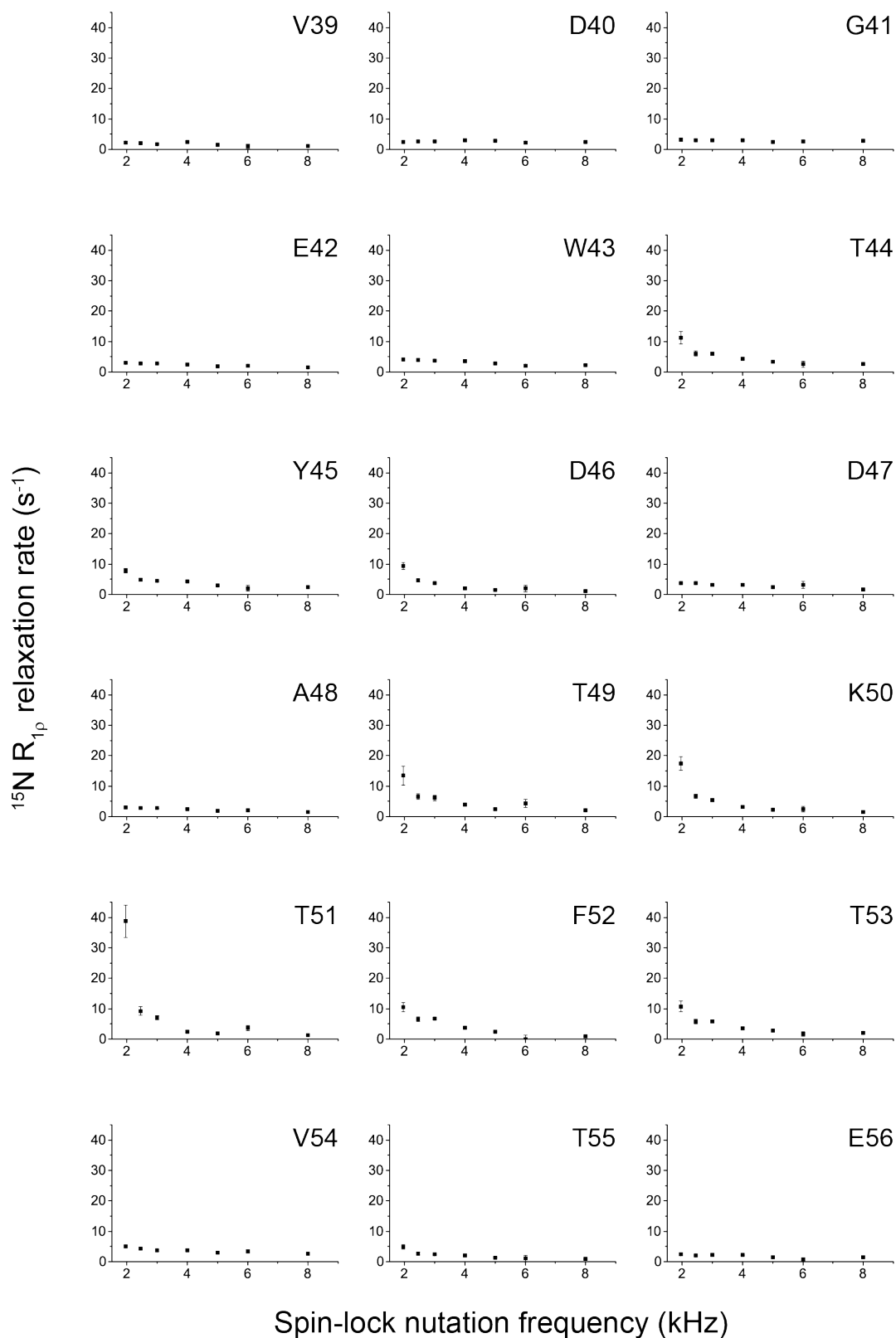


**Figure S5.**  $^{15}\text{N}$   $R_{1\rho}$  relaxation dispersion curves measured on crystalline 100% back-exchanged  $[\text{U-}^2\text{H}, ^{13}\text{C}, ^{15}\text{N}]\text{GB1}$  at a  $^1\text{H}$  Larmor frequency of 600 MHz, 50 kHz MAS and at a sample temperature of 27 °C. Spin-lock frequencies were determined by recording nutation experiments. While the majority of residues display little in the way of dispersion (i.e. most are flat), residues 17, 19, 20, 44, 46, 49, 50, 51, 52 and 53 show clear dispersion (displayed in Fig. 3b in the main manuscript). For those that are “flat”, the  $R_{1\rho}$  rate at a spin-lock field of 1.95 kHz is actually on average  $1.7\text{ s}^{-1}$  higher than the plateau value at 8 kHz spin-lock, an increase we attribute to the presence of coherent contributions to the measured rates at the lower spin-lock field.



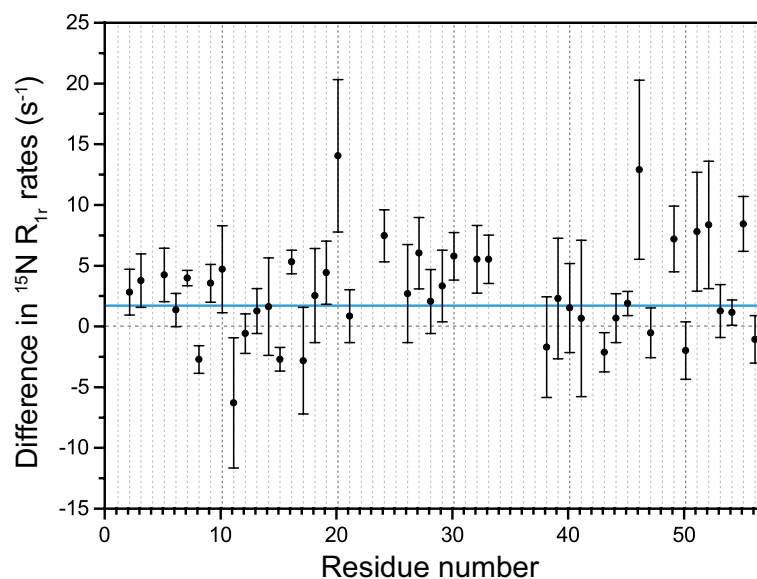
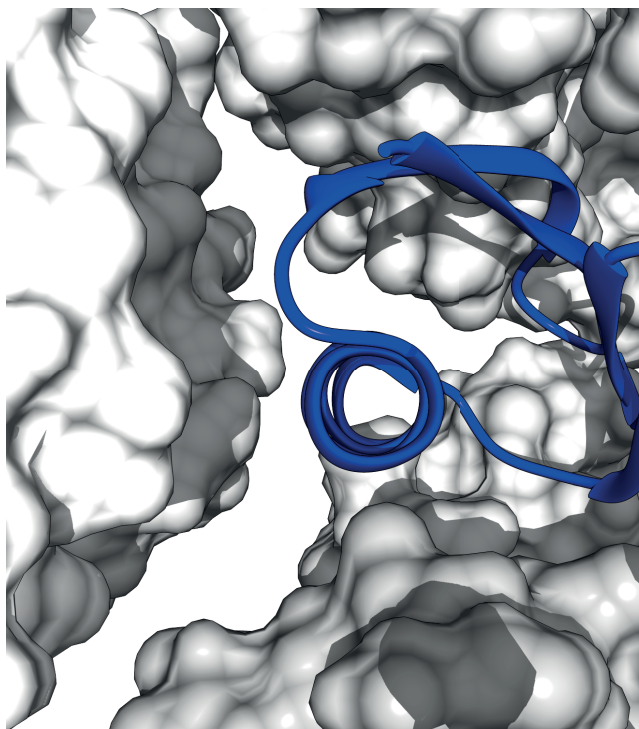


**Figure S6.** Differences between the  $^{15}\text{N}$   $R_{1\rho}$  relaxation rates measured at 2.5 kHz and 17 kHz spin-lock fields (i.e.  $R_{1\rho}[2.5\text{ kHz}] - R_{1\rho}[17\text{ kHz}]$ ) in 100% back-exchanged deuterated GB1 in complex with IgG, at a sample temperature of  $27 \pm 1$  °C. Exchange contributions are decoupled at 17 kHz, but at 2.5 kHz have observable effects on the decay rates. The horizontal blue line at  $1.7\text{ s}^{-1}$  represents the average coherent contribution to measured rates as found in crystalline deuterated GB1 at 50 kHz MAS and a spin-lock field amplitude of 1.95 kHz. While the latter conditions differ slightly from those used here (60 kHz MAS and 2.5 kHz spin-lock), this fact only ensures that  $1.7\text{ s}^{-1}$  is a safe overestimate of the coherent contribution in this case. All residues for which  $R_{1\rho}[2.5\text{ kHz}] - R_{1\rho}[17\text{ kHz}]$  is greater than this threshold by about one error bar or more (calculated from fit errors) were taken to be undergoing exchange processes on the  $\mu\text{s}$ -time scale (displayed in Fig. 3a in the main manuscript). These are residues 3-5, 7, 9, 10, 16, 19, 20, 24, 27, 30-31, 34, 36, 42, 46, 49, 51 and 52.

(a) crystal



(b) complex

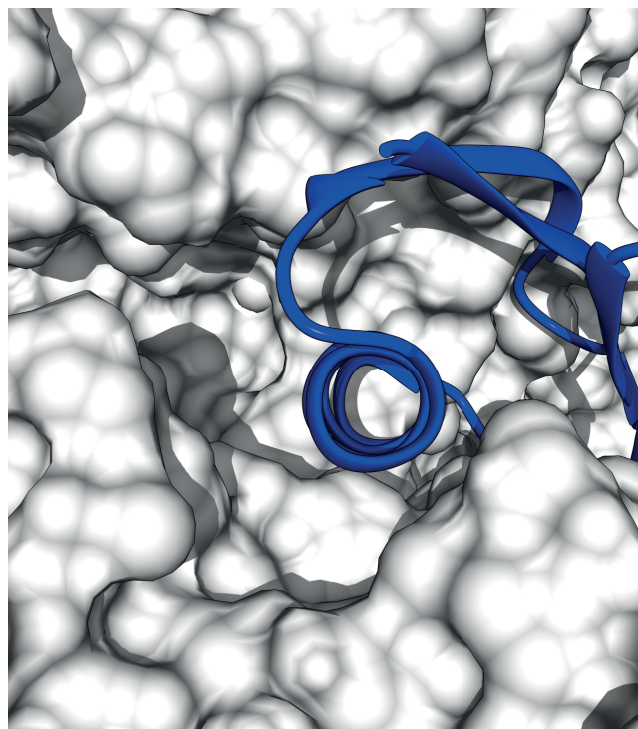


**Figure S7.** Comparison of helix packing in GB1 crystal (modeled using structure with PDB ID 2qmt<sup>[4]</sup>) and complex with IgG (modeled using structure of GB1 in complex with Fc fragment of IgG with PDB ID 1fcc;<sup>[6]</sup> our previous studies show that the interaction interface identified for a complex with a fragment is consistent with the interface in the complex with full length IgG). The buried surface area for the solvent accessible surface, calculated for the interface between the loop2-helix-loop3 fragment of GB1 and other molecules, is  $\sim 440 \text{ \AA}^2$  for the GB1 in the crystal and  $\sim 571 \text{ \AA}^2$  for GB1 in the complex. This indicates denser packing of the helix in the complex compared to in the crystal. Similarly, the buried surface area for the solvent accessible surface, calculated for the interface between the loop1-strand2-loop2 fragment of GB1 and other molecules,  $\sim 334 \text{ \AA}^2$  for the GB1 in the crystal and  $\sim 457 \text{ \AA}^2$  for GB1 in the complex (PDB ID 1igc<sup>[7]</sup> used as reference). The buried surface area was calculated in Chimera<sup>[3, 8]</sup> using models with added protons and deleted solvent molecules, ligands and ions.

### 3D GAF model including spinning frequency dependent expressions for $R_{1\rho}$

Single rigid-body motion is assumed and parameterized using a 3D GAF (Gaussian axial fluctuations) model where the coordinates of all NH vectors are expressed in a common molecular frame. As a starting point we expressed the NH vectors using polar coordinates in the inertia frame of GB1 (computed for the x-ray structure (PDB ID: 2qmt<sup>[4]</sup>)) and then used two angles to define the orientation of the reference frame as fit parameters. Thus the fit parameters included amplitudes of fluctuations against three orthogonal axes ( $\sigma_\alpha, \sigma_\beta, \sigma_\gamma$ ), a correlation time for the overall motion,  $\tau$ , and two angles  $\Delta\theta$  and  $\Delta\varphi$  defining the orientation of the reference frame for the motion (see below).

Fitting of the relaxation data (see Fig. 3a) to the model was performed in Matlab. The minimization was performed using code based on the *fminsearch* function with several random starting points to ensure a global minimum was found. The best-fit amplitude and time scale parameters for all the models were determined by minimizing the  $\chi^2$  target function:

$$\chi^2 = \sum_i \frac{(X_{i,calc} - X_{i,exp})^2}{\sigma_{i,exp}^2} \quad (11)$$

where  $X_i$  are relaxation rates,  $\sigma_i$  appropriate experimental errors.

Both dipolar NH ( $r_{NH} = 1.02 \text{ \AA}$ ) and  $^{15}\text{N}$  CSA (assuming axially symmetric CSA tensor collinear with NH vector;  $\Delta\sigma = -170 \text{ ppm}$ ,  $\eta = 0$ ) contributions to the relaxation were considered. The following expressions for relaxation rates were used:

$$R_{1\rho,N} = R_{1\rho,NH} + R_{1\rho,CSA}$$

$$R_{1\rho,NH} = \frac{1}{20} \left( \frac{\mu_0 \gamma_H \gamma_N}{2\pi \hbar r_{NH}^3} \right)^2 \left( \frac{2}{3} J_0(\omega_1 + 2\omega_r) + \frac{2}{3} J_0(\omega_1 - 2\omega_r) + \frac{4}{3} J_0(\omega_1 + \omega_r) + \frac{4}{3} J_0(\omega_1 - \omega_r) + 3J_1(\omega_N) + J_0(\omega_H - \omega_N) + 6J_1(\omega_H) + 6J_2(\omega_H + \omega_N) \right)$$

$$R_{1\rho,N,CSA} = \frac{1}{45} (\sigma_{\parallel} - \sigma_{\perp})^2 \left( \frac{2}{3} J_0(\omega_1 + 2\omega_r) + \frac{2}{3} J_0(\omega_1 - 2\omega_r) + \frac{4}{3} J_0(\omega_1 + \omega_r) + \frac{4}{3} J_0(\omega_1 - \omega_r) + 3J_1(\omega_N) \right)$$

The above expressions for  $R_{1\rho}$  are based on the expressions from ref. [9] considering an on-resonance  $R_{1\rho}$  measurement.

The spectral density was defined as:

$$J(\omega) = (1 - S_{\mu\nu}^2) \frac{\tau}{1 + (\omega\tau)^2}$$

with the 3D GAF order parameter  $S_{\mu\nu}^2$  being defined as:

$$S_{\mu\nu}^2 = \frac{4\pi}{5} \sum_{l,k,k',m,m'=-2}^2 (-i)^{k-k'} e^{-\frac{\sigma_\alpha^2}{l^2} - \frac{\sigma_\beta^2(k^2+k'^2)}{2} - \frac{\sigma_\gamma^2(m^2+m'^2)}{2}} d_{kl}^{(2)}\left(\frac{\pi}{2}\right) d_{k'l}^{(2)}\left(\frac{\pi}{2}\right) d_{m'k'}^{(2)}\left(\frac{\pi}{2}\right) Y_{2m}(\mathbf{e}_\mu^{pp}) Y_{2m'}^*(\mathbf{e}_\nu^{pp})$$

where  $Y_{2m}$  are the second spherical harmonics and  $\mathbf{e}_\mu^{pp} = (\theta_\mu, \varphi_\mu)$  defines the principal axis for the interaction  $\mu$  in the 3D GAF reference frame for the motions.<sup>[10]</sup>  $d_{kl}^{(2)}(\frac{\pi}{2})$  are the reduced Wigner matrix elements with the rotation angle in the parenthesis.  $\sigma_\alpha, \sigma_\beta, \sigma_\gamma$  are the fluctuations (in rad) against three orthogonal axes  $\alpha, \beta, \gamma$ .

For very slow motions the contributions to  $^{15}\text{N}$   $R_{1\rho}$  from fluctuations of dipolar couplings between nitrogens and protons that are not directly bonded to them (including protons on IgG) may be non-negligible. By considering x-ray structures of GB1 analogues with IgG fragments we estimated that typically the cumulative effect of such couplings should not exceed the effective coupling corresponding to a distance of  $\sim 2.5 \text{ \AA}$ . In order to evaluate how such contributions would influence the above 3D GAF analysis we refitted the data including an additional term for all the residues corresponding to relaxation induced by  $2.5 \text{ \AA}$  NH dipolar relaxation. The isotropic  $S^2$  for this contribution was treated as an additional fit parameter. In order to avoid solutions that may violate assumptions of Redfield theory we have also imposed an additional penalty for correlation times that approach the largest relaxation rates. The best fit yielded fluctuations of  $3.1^\circ, 5.3^\circ, 5.6^\circ$  with  $\Delta\theta = 11.8^\circ, \Delta\varphi = 14.7^\circ$  (i.e. axes similar to the ones presented in Fig. 3), with a correlation time of  $\tau = \sim 54 \text{ \mu s}$  and  $S^2 = 0.999$ .

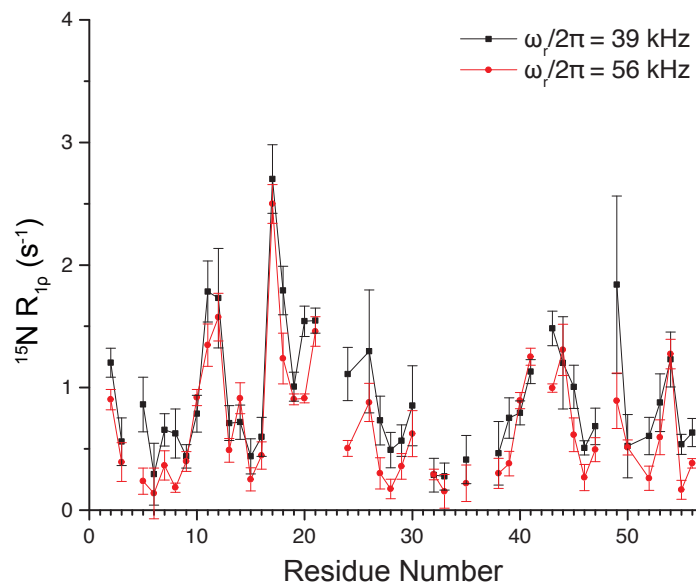


**Figure S8.** Comparison of  $^{15}\text{N}$   $R_{1\rho}$  rates measured at 56 and 39 kHz spinning frequencies measured for crystalline 100%  $\text{H}_2\text{O}$  [ $^2\text{H}$ ,  $^{13}\text{C}$ ,  $^{15}\text{N}$ ]GB1 at  $\omega_{1\text{N}}/2\pi = 10$  kHz, 600 MHz  $^1\text{H}$  Larmor frequency with a sample temperature of  $27 \pm 1$  °C.

## References

- [1] W. T. Franks, D. H. Zhou, B. J. Wylie, B. G. Money, D. T. Graesser, H. L. Frericks, G. Sahota, C. M. Rienstra, *J. Am. Chem. Soc.* **2005**, *127*, 12291-12305.
- [2] J. R. Lewandowski, J. Sein, H. J. Sass, S. Grzesiek, M. Blackledge, L. Emsley, *J. Am. Chem. Soc.* **2010**, *132*, 8252-8254.
- [3] E. F. Pettersen, T. D. Goddard, C. C. Huang, G. S. Couch, D. M. Greenblatt, E. C. Meng, T. E. Ferrin, *J. Comp. Chem.* **2004**, *25*, 1605-1612.
- [4] H. L. Frericks Schmidt, L. J. Sperling, Y. G. Gao, B. J. Wylie, J. M. Boettcher, S. R. Wilson, C. M. Rienstra, *J. Phys. Chem. B* **2007**, *111*, 14362-14369.
- [5] D. B. Good, S. Wang, M. E. Ward, J. Struppe, L. S. Brown, J. R. Lewandowski, V. Ladizhansky, *J. Am. Chem. Soc.* **2014**, *136*, 2833-2842.
- [6] A. E. Sauer-Eriksson, G. J. Kleywegt, M. Uhlen, T. A. Jones, *Structure* **1995**, *3*, 265-278.
- [7] J. P. Derrick, D. B. Wigley, *J. Mol. Biol.* **1994**, *243*, 906-918.
- [8] M. F. Sanner, A. J. Olson, J. C. Spehner, *Biopolymers* **1996**, *38*, 305-320.
- [9] R. Kurbanov, T. Zinkevich, A. Krushelnitsky, *J. Chem. Phys.* **2011**, *135*, 184104.
- [10] S. F. Lienin, T. Bremi, B. Brutscher, R. Bruschweiler, R. R. Ernst, *J. Am. Chem. Soc.* **1998**, *120*, 9870-9879.